An Isentropic Mesoα-Scale Analysis System and Its Sensitivity to Aircraft and Surface Observations

STANLEY G. BENJAMIN

Program for Regional Observing and Forecasting Services (PROFS), NOAA Environmental Research Laboratories, Boulder, Colorado and National Center for Atmospheric Research, Boulder, Colorado*

(Manuscript received 20 October 1988, in final form 5 January 1989)

ABSTRACT

An objective analysis scheme for meteorological variables on constant potential temperature surfaces is presented. The analysis uses a form of multivariate statistical interpolation and is designed to retain mesoscale detail in disparate observations including rawinsonde, surface, aircraft, satellite, and wind profiler data while combining them with a forecast background (first guess) field. The wind and mass field analyses are interdependent. The horizontal correlation of forecast error on isentropic surfaces is modeled with an analytical function from statistics collected for this study; the vertical correlation of forecast error is modeled as a function of potential temperature separation. These correlations determine the weights applied to observed-minus-forecast increments in the analysis. The analysis is two-dimensional except with respect to single-level data where it is three-dimensional.

Comparisons of isentropic and isobaric analyses are shown, and examples of the effects of single-level (aircraft and surface) observations on isentropic analyses are presented. Although variable in space and time, these datasets are often of higher density than the rawinsonde network, and they support increased resolution of mesoscale features in the analysis. More importantly, the examples reveal that three-dimensional analysis increment structures, especially in the vicinity of fronts, appear to be more physically reasonable in an isentropic analysis than in an isobaric analysis.

1. Introduction

Although the analysis and initialization problem is important for numerical weather prediction in general, it is particularly crucial for very short range (0–12 h) numerical forecasts. Anthes et al. (1982) have demonstrated that a high-resolution mesoscale model with good boundary-layer and precipitation parameterizations and a detailed specification of terrain and surface characteristics can simulate many mesoscale features by 12–24 h, even when initialized with synoptic-scale data. But in order to obtain a useful forecast (before the events actually occur) in less time, the model initial state must already have incorporated these features to some extent. The relative contributions of observations (initial conditions) versus models toward forecast skill as a function of time is subjectively depicted in a figure by Anthes and Baumhefner (1984); observations are relatively more important than model physics for short-range forecasts and less important at longer ranges.

Aiming toward better mesoscale analyses, researchers such as LeDimet and Talagrand (1986) and Derber (1987) have pioneered in the use of the adjoint model method. In this method, an analysis is produced by combining a four-dimensional set of observations subject to the constraint of the equations of an NWP model, but the technique is extremely time consuming by today's computational standards. Operational implementation is not likely for several years.

A much simpler approach, coordinate transformation, currently remains a relatively unexplored area for improving the accuracy of mesoscale analyses. This paper describes an isentropic coordinate analysis that is part of the Mesoscale Analysis and Prediction System (MAPS) developed at the Program for Regional Observing and Forecasting Services (PROFS) to provide real-time guidance for forecasters.

Rossby (1937) first summarized the advantages of viewing weather features on isentropic surfaces: that isentropic surfaces act like material surfaces, that flow patterns on them are spatially and temporally coherent, and that frontal discontinuities are virtually nonexistent. Thus, baroclinic zones are better resolved on isentropic surfaces than on isobaric surfaces, as are features produced by advective processes along quasi-ma-

* The National Center for Atmospheric Research is sponsored by the National Science Foundation.

Corresponding author address: Dr. Stanley G. Benjamin, NOAA/ERL, 325 Broadway, Boulder, CO 80303-3328.

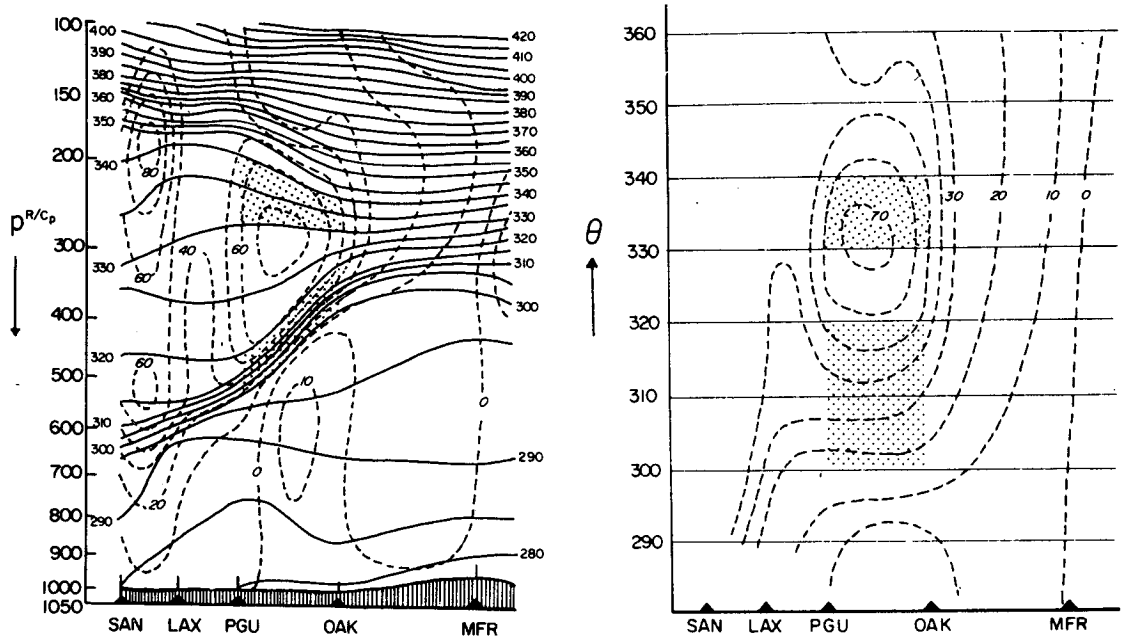

FIG. 1. Comparison of resolution in isobaric and isentropic coordinates for a cross section of wind speed through a frontal zone. Solid lines are isentropes and dashed lines are isotachs (m s^{-1}). From Bleck and Shapiro (1976) and Shapiro and Hastings (1973).

terial isentropic surfaces. Isentropic analyses have been used to particular advantage in studies of three-dimensional flow around cyclones (e.g., Danielsen and Bleck 1967; Carlson 1980; Uccellini et al. 1987) and fronts (e.g., Reed and Sanders 1953; Sanders 1955).

These characteristics are also very advantageous for the objective analysis problem, because the usual analysis assumption of isotropic, or even along-flow anisotropic influence of observations appears to be quite well founded in isentropic coordinates. A comparison of cross sections through a front in isobaric and isentropic coordinates (Fig. 1) produced by Bleck and Shapiro (1976) and Shapiro and Hastings (1973) shows how the vertical and horizontal scale of some features (in this case, a frontal zone) can be enlarged in the isentropic perspective.

Several different approaches to objective analysis in isentropic coordinates have been developed in the last 15 years. Primary among them is that developed by Bleck (1975) who used a statistical interpolation technique to combine Montgomery stream function ($M = C_pT + gz$) and wind observations into an analysis of M. A more recent, concerted effort toward isentropic analysis (Andersson et al. 1986) is now ongoing at the Swedish Meteorological and Hydrological Institute (SMHI). A variational approach to isentropic analysis of the mass field was used by Buzzi et al. (1985), and Mancuso et al. (1981) used an isentropic station selection scheme for an isobaric successive-correction analysis. An innovative approach to three-dimensional analysis using isentropic cross sections was reported by Petersen (1986).

The MAPS isentropic analysis reported here is similar to the SMHI scheme but different from others in that it is multivariate in Montgomery streamfunction M and wind (u, v), and observations are combined with background fields from an external forecast model. The MAPS analysis incorporates data not only from rawinsondes, but also from surface-based wind profilers, aircraft reports, surface observations, and soon, satellite radiance information. The use of single-level data in the MAPS analysis is unique for isentropic objective analyses and has been an important goal in its development.

After a description of the MAPS domain in section 2, the incorporation of each observation type into the MAPS isentropic analysis is treated in section 3. Section 4 deals with the background field and its statistical properties, including the horizontal and vertical correlation of forecast error in isentropic coordinates. The analysis technique itself is discussed in section 5. Two different comparisons between isentropic and isobaric analyses are presented in section 6, and examples of the influence of aircraft and surface data are provided in section 7. A summary in section 8 concludes the paper.

2. Analysis domain

The analysis domain for the experiments described here covers the contiguous United States and neigh-

boring regions with a 42 × 32 grid with a 111-km grid-length, adequate to resolve most but not all mesoα scale wavelengths (200–2000 km). There are 12 isentropic analysis surfaces at 255, 265, 275, 285, 295, 305, 315, 325, 335, 350, 365, and 395 K. Thus, the vertical resolution is 10 K for the troposphere, and widens in the stratosphere. All these levels are effectively used in winter, but the lowest 3–5 potential temperatures usually are not found over this domain during the summer. This horizontal and vertical resolution was dictated by computer limitations at PROFS and real-time application of the analysis scheme.

Strictly speaking, the MAPS analysis scheme is performed on surfaces of constant *virtual* potential temperature (θ_v), since water vapor is approximately accounted for in hydrostatic calculations. For the rest of this paper, θ will represent θ_v and the term "isentropic" will be understood to refer to a surface of constant θ_v.

3. Treatment of observations

The analysis variables are M/g, u, v (M/g, u, and v have the same geostrophic relationship as z, u and v in isobaric coordinates), p (pressure) and RH* ($= \sqrt{1 - \text{RH}}$) (Rasmussen 1982), where RH is relative humidity. The moisture analysis variable is being changed in the next version of the scheme to the condensation pressure, a quantity which is conserved with flow on isentropic surfaces in the absence of evaporation or condensation.

a. *Types of observations*

Both profile and single-level data are used within this isentropic analysis system. The types of data and their typical volumes as of this writing are shown in Table 1. Special preprocessing is needed for each observation type.

1) RAWINSONDE

Vertical profiles of wind and moisture from rawinsondes are linearly interpolated using the Exner function

$$\Pi = C_p\left(\frac{P}{P_0}\right)^{R/C_p}, \qquad (1)$$

where P_0 = 100 kPa, to the correct virtual potential temperature levels. Profiles of M are determined by integrating the hydrostatic relationship,

$$\frac{\partial M}{\partial \theta} = \Pi, \qquad (2)$$

upwards. Danielsen (1959) found that determining M in this manner avoids errors produced by separately interpolating gz and C_pT.

2) PROFILER

Since wind profiler observations are determined as a function of height, an external data source is needed to allow mapping from height to potential temperature. The MAPS system currently uses three-dimensional gridded data from the Nested Grid Model (NGM) run at the National Meteorological Center (NMC). Vertical profiles are again linearly interpolated in Π to the analysis isentropic levels. The external data source is being changed to forecasts from the MAPS isentropic assimilation system.

3) AIRCRAFT

Aircraft observations often contain both a temperature and a wind observation along with a flight level that, above 19 000 feet altitude, corresponds to a pressure determined from the standard atmosphere. Thus, if an aircraft report contains a temperature, the potential temperature is also known. If not, gridded data from the NGM (or MAPS) are again used to determine the potential temperature that corresponds to the reported flight level. A virtual temperature correction is made for aircraft data, using RH information from the NGM. Aircraft reports of icing are converted into proxy observations of 100% relative humidity.

4) SURFACE

In this scheme, surface aviation observations are directly incorporated into the three-dimensional isentropic analysis to provide more detail in the vicinity of the intersection of isentropes with the surface. Surface observations are checked for accuracy against each other using a 1-h persistence from a previous surface analysis (Miller and Benjamin 1988) as a background. A surface superobservation is produced for each grid volume that contains more than one surface station.

TABLE 1. Observations available for use in MAPS isentropic analysis.

	Approximate volume in MAPS domain	Variables used in analysis
Rawinsonde	75 stations	M, p, u, v, RH
Profiler	4 stations (all in Colorado)	u, v
Aircraft	400 per 3-h window—1200 UTC 1000 per 3-h window—0000 UTC	p, u, v, RH
Surface	900	p, u, v, RH
Satellite (not used for this paper)	600–900 soundings	thickness

The superobservation contains a mean value of surface pressure (determined from altimeter setting), potential temperature, RH, and the horizontal wind components, and is positioned at the centroid location. The number of observations combined is retained to allow the reduction of the specified observation error later in the analysis program, but this reduction is not being done currently.

Surface observations can only be used in isentropic analysis if the station pressure can be determined. This is possible with most North American surface aviation observations since they usually include an altimeter setting, but unfortunately, not with surface synoptic reports.

5) SATELLITE

Experiments performed at PROFS (Benjamin et al. 1988) suggest that a safe but effective method to include satellite mass information within an analysis over a data-rich region is to adjust the background fields to agree with mass gradients indicated by satellite radiances. Thus, in situ observations incorporated in the subsequent analysis are allowed to take precedence over satellite data where a discrepancy exists. This method is currently being implemented in the isentropic version of MAPS and was not used for the examples shown in this paper. For the isentropic analysis, increments to the mass field and corresponding geostrophic wind increments are determined in isobaric coordinates and are then interpolated to isentropic coordinates. To reduce the error from vertical interpolation, only the increments are interpolated rather than the full fields.

b. Quality control of observations

Vertical quality control checks for reasonable shear, stable lapse rate, and hydrostatic consistency are first performed on rawinsonde profiles consisting of both mandatory and significant level data. These checks are identical to those done in the pressure coordinate version of MAPS (Benjamin et al. 1985). In the isentropic version, the sounding is adjusted to ensure a weakly stable lapse rate (1 K potential temperature per 100 mb). When a superadiabatic layer is detected that is not due to an obvious temperature error at one level or the other, the temperature at the lower level is always adjusted to ensure weak stability. Because the superadiabatic layer near the surface often found in 0000 UTC soundings in North America is usually quite shallow compared with the depth of the surface mixed layer, there is usually less energy change if θ is adjusted from the top down rather than from the bottom up. This same adjustment cannot be done with surface observations since they are single-level. A post-analysis check, however, is also performed to ensure at least a weakly stable monotonic increase of potential temperature with height; as with temperature soundings, this adjustment is done "top down."

Horizontal quality control is performed on isentropic surfaces, one variable at a time, via optimal interpolation. Differences between observations and the background are interpolated to each observation point (a "buddy check"). Subtracting out the background field improves error dectection. The difference between this estimated value and the actual observed-minus-background value is used to make a quality control judgment. The error threshold allowed is a function of the expected analysis error (a by-product of optimal interpolation; Gandin 1963), which depends upon the location and error characteristics of surrounding observations.

An optional interactive graphics system allows a user to review the results of the objective quality control and revise those decisions, if deemed necessary. This quality control system is very similar to that described in Benjamin et al. (1985) but has been reconfigured in isentropic coordinates. The expected advantage of improved field coherence in isentropic coordinates has been noted in several cases where observations (particularly those of relative humidity) were flagged in the pressure–coordinate system but retained in the isentropic system.

TABLE 2. Observational error standard deviations used in MAPS isentropic analysis.

Rawinsonde observational errors								
Pressure (mb)	Height (m)	u, v components (m s^{-1})	Other wind observations (m s^{-1})		RH* observations (nondimensional)		Temperature observations (K)	
850	6.4	0.8	Aircraft	1.5	Rawinsonde	0.05	Rawinsonde	0.4
700	6.9	0.9	Profiler	1.5	Aircraft	0.10	Aircraft	2.0
500	9.7	0.9	Surface	4.0	Surface	0.07	Surface	0.8
400	11.9	1.0						
300	15.0	1.1						
250	20.3	1.2						
200	22.2	1.2						
150	25.9	1.4						

TABLE 3. Background error standard deviations used in MAPS isentropic analysis.

Pressure (mb)	Height		Temperature		RH*		Winds (m s^{-1})	
	Summer (m)	Winter (m)	Summer (K)	Winter (K)	Summer	Winter	Summer m s^{-1}	Winter m s^{-1}
850	15.0	21.6	2.7	2.7	0.13	0.175	3.3	3.8
700	16.8	22.0	1.8	2.0	0.16	0.17	3.2	3.8
500	21.0	23.3	1.2	1.5	0.19	0.17	3.5	4.7
400	25.2	27.4	1.3	1.8	0.19	0.17	4.2	5.7
300	30.2	31.6	1.7	2.4	0.19	0.17	4.8	6.5
250	32.7	33.2	1.9	2.6	0.19	0.17	5.4	6.9
200	35.8	35.8	1.8	2.5	0.19	0.17	4.5	6.5
150	39.0	38.4	1.7	2.4	0.19	0.17	3.7	5.5

c. *Superobservations*

"Superobservations" are created through linear combination of any observations separated by 25 km or less. A weighting matrix based upon observation error of each data type for each variable keeps the most reliable observation or averages for equally reliable observations. This operation prevents ill-conditioned covariance matrices and provides an estimate of the true value that is statistically superior to any of the original observations. Single-level observations may be combined with each other, but can be combined with station profiles only if the θ difference is less than 0.5 K. Otherwise, single-level observations within 25 km of profile observations are discarded.

d. *Specification of observation error*

The specification of observation error allows optimal interpolation to control how closely the analysis fits different observations (e.g., Gandin 1963). The observation error is a function of both measurement error and unrepresentativeness (sampling) error, but the present scheme does not differentiate between these two. The values used in the MAPS isentropic analysis are shown in Table 2. Since the change of error with height is better described as a function of pressure than of potential temperature, a look-up table in the analysis determines the observation error by the mandatory level nearest to the observation. The values used are similar to those used in the Regional Analysis and

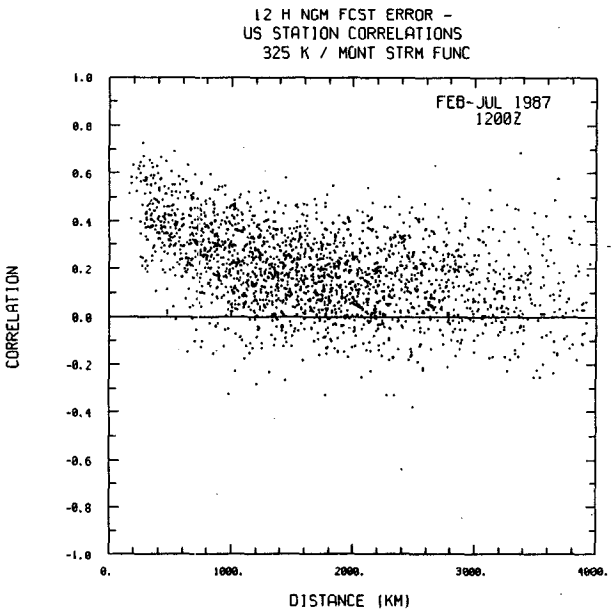

FIG. 2. Scatter diagram of station–station correlations for 325 K (M/g) observed-minus-forecast differences as a function of horizontal distance. Forecast is 12-h Nested Grid Model forecast.

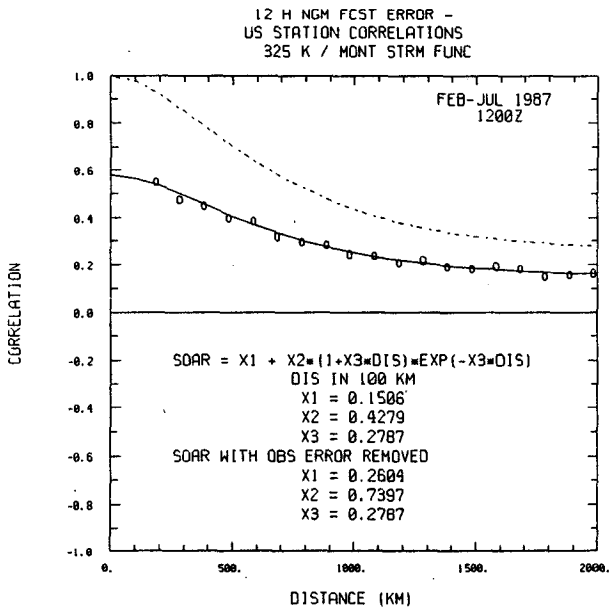

FIG. 3. Horizontal correlation of 325 K (M/g) observed-minus-forecast differences. Same as Fig. 2, except that circles are distance-binned correlations and solid lines are fits of SOAR functions to points. Solid line includes effect of observational error and dashed line has observational error removed.

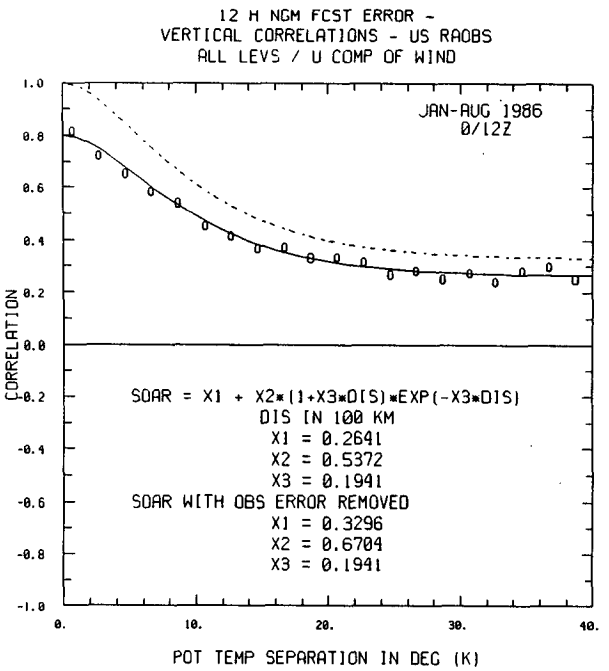

FIG. 4. Vertical correlation of u observed-minus-forecast differences as a function of potential temperature separation. Forecast is 12-h Nested Grid Model forecast.

Forecast System (RAFS, which includes the Nested Grid Model) developed at NMC (DiMego 1988) but smaller than those used in the NMC Global Data Assimilation System (Dey and Morone 1985). This reduction of observation error accounts for the likelihood that the error of unrepresentativeness is decreased with a smaller mesh size. The next version of MAPS will allow distinction between automated and voice-reported aircraft reports.

The spatial correlation of observational error does not need to be accounted for in this analysis. The analysis scheme is two-dimensional (horizontal) with respect to all profile data (rawinsonde and profiler); it is three-dimensional (using vertical correlations) only with respect to single-level data and to top-level rawinsonde wind observations when upper tropospheric winds carry the balloon too close to the horizon for accurate determination of wind speed.

TABLE 4. Horizontal correlation of 12-h NGM forecast error on isentropic surfaces—parameters for fits of second-order autocorrelation functions.

	R_{oo}	R_o	c
Montgomery streamfunction			
285 K	0.05	0.95	0.33 × $(10^5$ km$)^{-1}$
305 K	0.30	0.70	0.23
325 K	0.27	0.73	0.35
350 K	0.12	0.88	0.23
Pressure			
285 K	0.02	0.98	0.52
305 K	0.30	0.70	0.39
325 K	0.24	0.76	0.30
350 K	0.14	0.86	0.24
RH*			
285 K	0.16	0.84	0.30
305 K	0.08	0.92	0.45
325 K	0.08	0.92	0.40
350 K	0.08	0.92	0.40

4. Treatment of background

Through July 1988, gridded data from the National Meteorological Center's Nested Grid Model have been interpolated to isentropic coordinates and used as the background for the real-time MAPS isentropic analysis. Winds and relative humidity are interpolated linearly in the vertical as a function of Exner function (Π). Montgomery streamfunction and Exner function on isentropic surfaces are determined from isobaric height and temperature data using Hermite polynomials, with the hydrostatic relationship in isentropic coordinates [Eq. (2)] as a constraint. All horizontal interpolation from the NGM grid used for transmission (1.25° lat × 2.5° long, coarser than the original 91 km NGM "C" grid) to MAPS grid points is accomplished by bicubic Hermite polynomials.

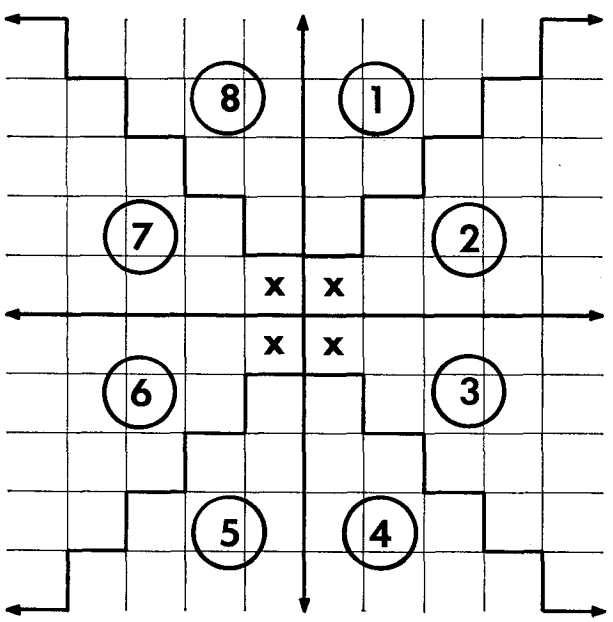

FIG. 5. Observation search sectors for the four-point volume method. The four grid points for which an analysis is to be made are marked by ×. Grid volumes in each sector are searched with increasing distance from the center until a grid volume is found that contains a report.

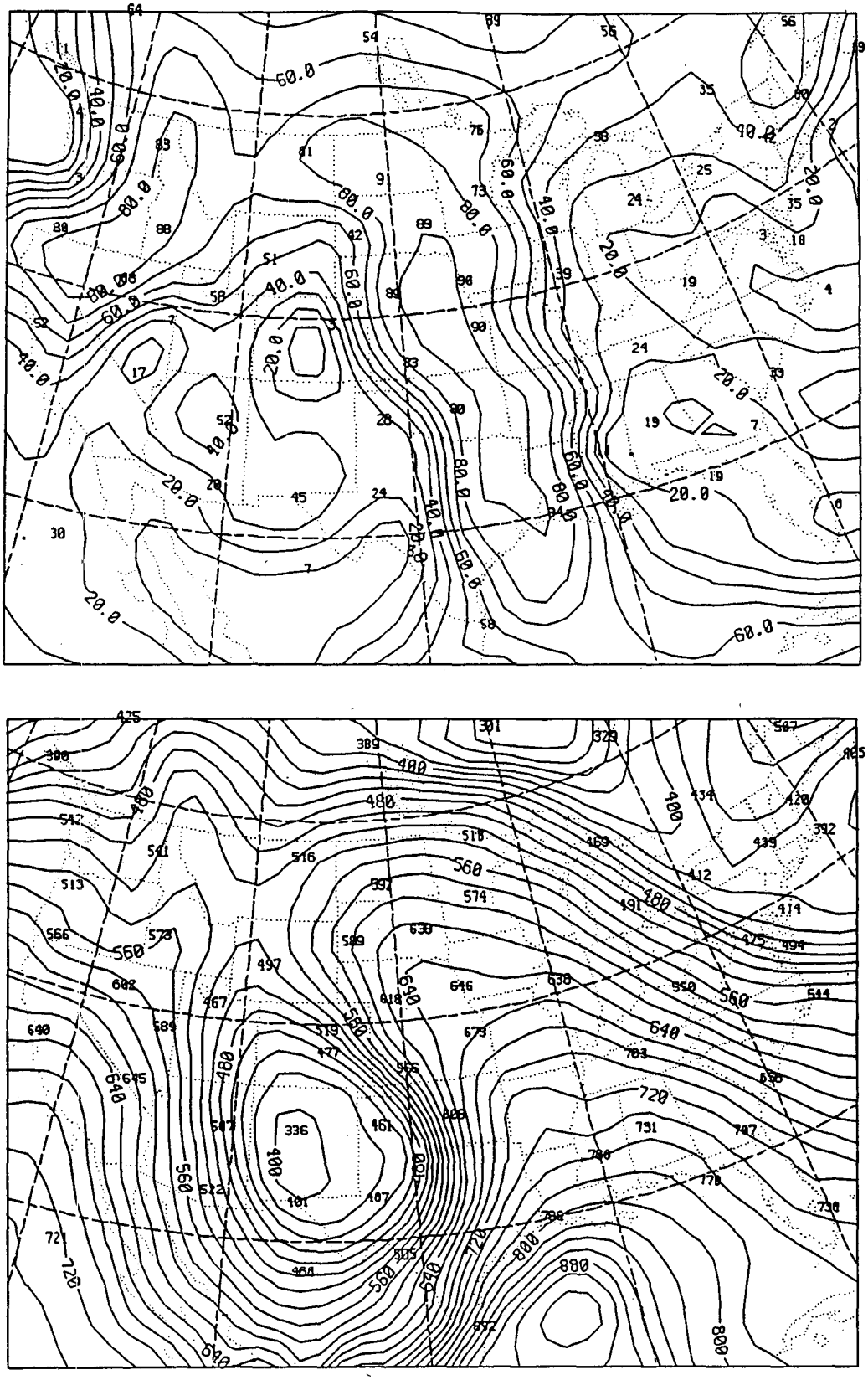

FIG. 6. (a) Relative humidity analysis at 305 K for 1200 UTC 17 March 1987, (b) pressure analysis at 305 K for same time, and (c) relative humidity analysis at 500 mb for same time. In (a)–(c), observations are plotted in small characters.

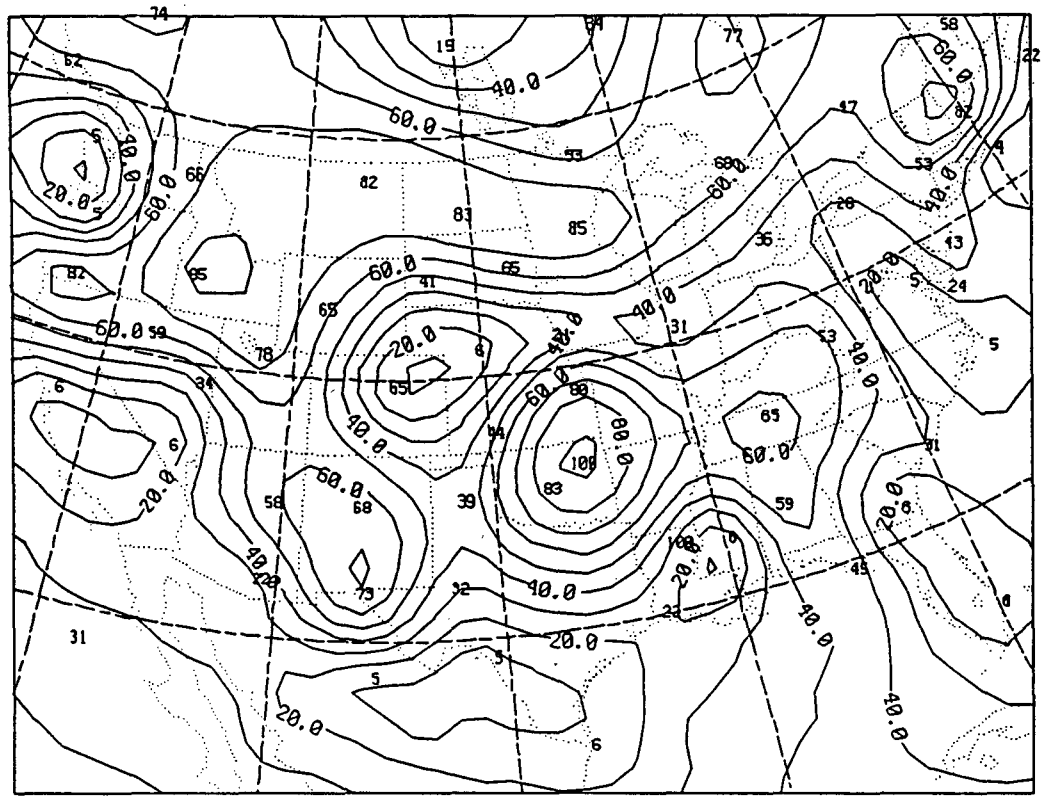

FIG. 6. (*Continued*)

Since July 1988, the background for the analysis has been forecast fields from the MAPS isentropic primitive equation model (Brümmer 1987). Initial results from the MAPS data assimilation cycle in isentropic coordinates will be reported in a future paper.

a. Background error standard deviation

The values for background error standard deviation are specified by season from 12-h forecast error statistics compiled by the National Meteorological Center for the Limited-area Fine-Mesh (LFM) model for January and July 1985. These values are listed in Table 3. Like observation errors, the background errors are specified as a function of the local pressure for each observation used in the isentropic analysis.

b. Horizontal correlation of background error

To determine horizontal correlation of background error, a 6-month collection (February–July 1987) was made of 12-h forecast errors on isentropic surfaces from the NGM. Data were collected for 70 rawinsonde stations in the United States; 2415 pairs were obtained from which forecast error covariances could be calculated. These covariances were normalized by the total variances at each station within a given pair to determine correlations. Observations which did not pass the quality control checks (section 3b) were not used, and if any levels of NGM gridded data were missing or showed possible transmission errors, that observation time was discarded. The calculated correlations include the error produced by vertical interpolation from isobaric to isentropic surfaces. A direct interpolation from sigma to isentropic surfaces of NGM output would probably produce slightly different correlations, but the correlations calculated are appropriate for this analysis since sigma-level data from the NGM are unavailable.

The correlations themselves show considerable scatter (Fig. 2), typical for forecast error statistics and reflecting the fact that no single structure function (or weighting function for nonstatistical interpolation schemes) will be appropriate for all situations or even for all pairs of stations. To prepare for fitting a model to these points, the correlations were grouped according to separation distance in bins 100 km wide, i.e., 100–200 km, 200–300 km, etc. The analytical model chosen was the second-order autoregressive (SOAR) function (Thiébaux 1985):

$$\mu(s) = R_{00} + R_0(1 + cs)e^{-cs}, \qquad (3)$$

where s is distance in kilometers, and R_{00}, R_0, and c are constants. SOAR functions were fit to the bin-av-

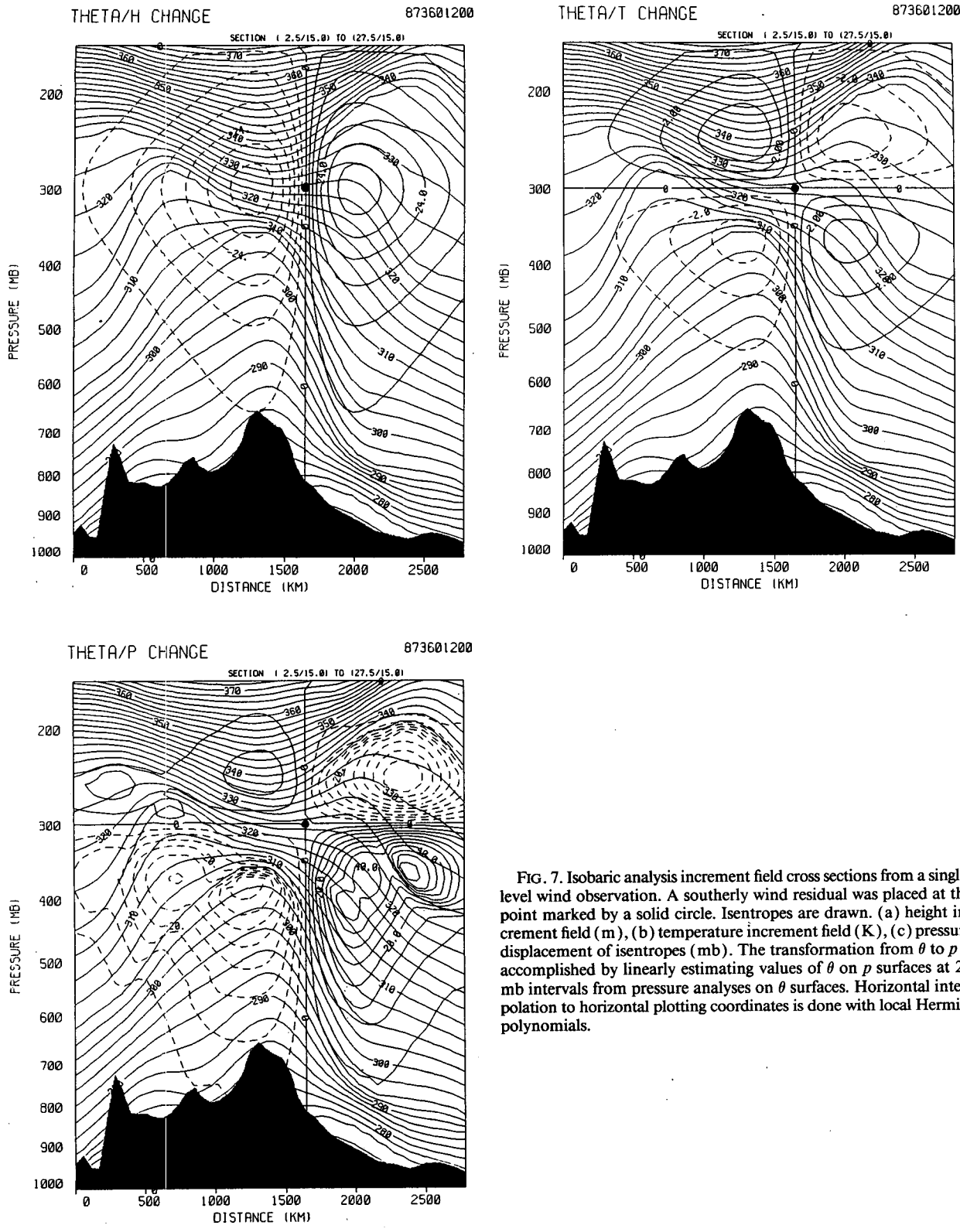

FIG. 7. Isobaric analysis increment field cross sections from a single-level wind observation. A southerly wind residual was placed at the point marked by a solid circle. Isentropes are drawn. (a) height increment field (m), (b) temperature increment field (K), (c) pressure displacement of isentropes (mb). The transformation from θ to p is accomplished by linearly estimating values of θ on p surfaces at 20 mb intervals from pressure analyses on θ surfaces. Horizontal interpolation to horizontal plotting coordinates is done with local Hermite polynomials.

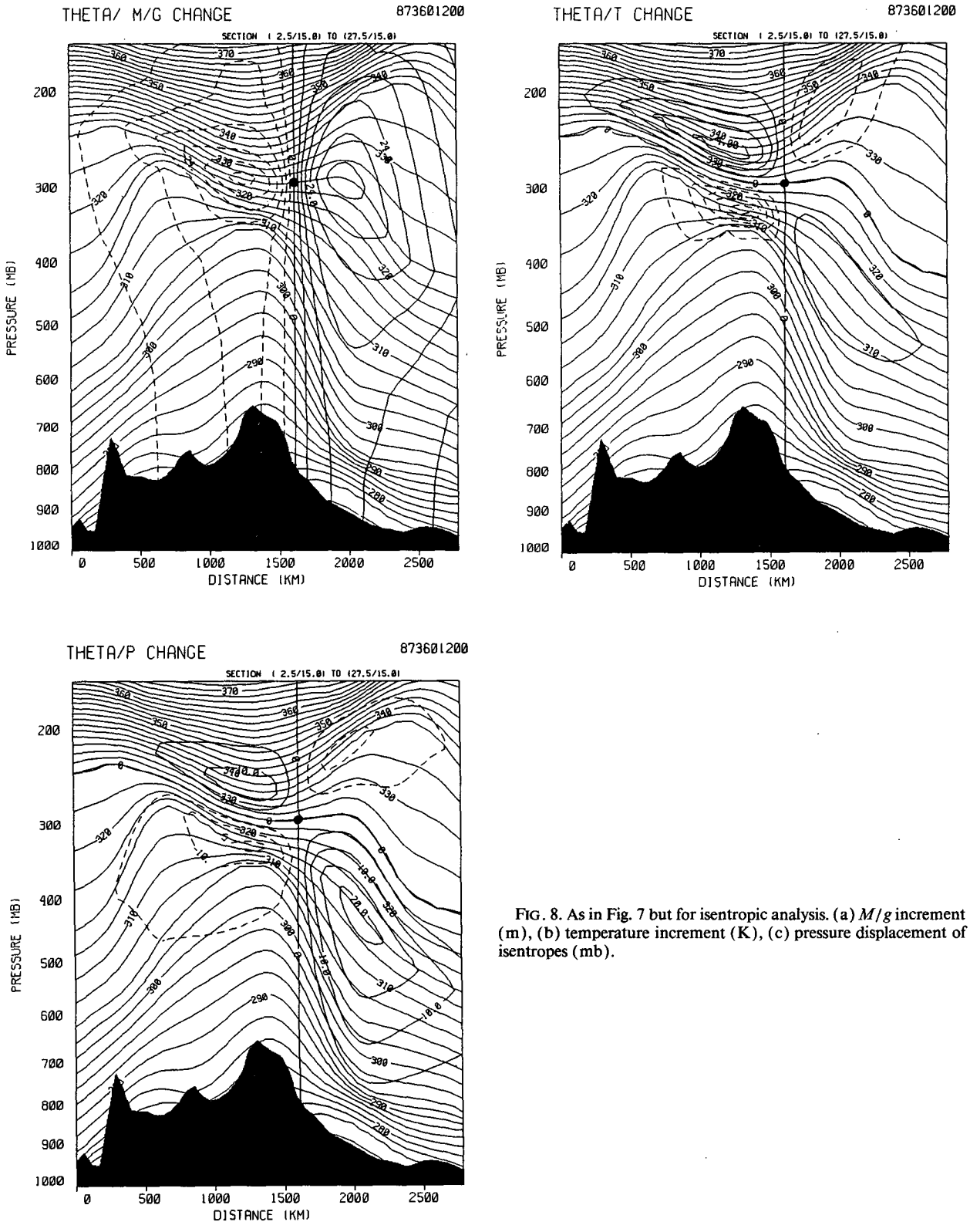

FIG. 8. As in Fig. 7 but for isentropic analysis. (a) M/g increment (m), (b) temperature increment (K), (c) pressure displacement of isentropes (mb).

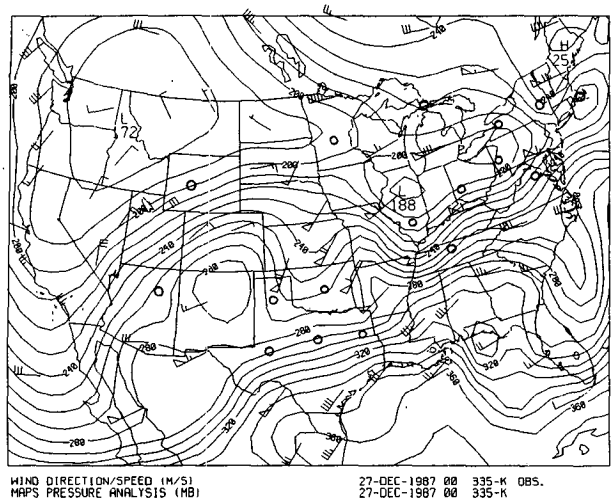

FIG. 9. Rawinsonde wind observations and pressure analysis for 335 K isentropic surface, 0000 UTC 27 December 1987. Open circles represent missing rawinsonde wind observations. Solid flag = 50 m s^{-1} (100 kt).

erage correlations using the least-squares Levenberg–Marquardt algorithm (Thiébaux et al. 1986). For each set of data, a zero-intercept was determined that represented the relative contribution of observational (measurement and unrepresentativeness) error versus forecast error (Rutherford 1972, Lönnberg and Hollingsworth 1986). New curve-fits were then calculated (Fig. 3—dashed) with correlations rescaled using this ratio such that the new zero-intercept were equal to 1; this removes the influence of observational error (Gandin 1963). The three- parameter form of the SOAR function allows a better fit over a limited range (≤2000 km); the mean correlation in Fig. 2 appears to approach zero beyond 2000 km. SOAR function parameters were determined for Montgomery streamfunction, pressure and RH* at 4 different isentropic levels (Table 4). Values at other levels were then determined by interpolation. Curve-fits were determined independently for 1200 and 0000 UTC data and then averaged to avoid contamination from the diurnal cycle, a complication for M and p statistics. The values of c for Montgomery streamfunction are similar to those found by Thiébaux et al. (1986) for height forecast errors from the operational Canadian forecast model. Forecast error on isentropic surfaces of RH is generally of a smaller scale (indicated by a larger c) than that of mass variables (Table 4).

A second collection of forecast error statistics, now underway at PROFS, will allow a comparison of horizontal correlations in isentropic versus isobaric coordinates. Seaman and Gauntlett (1982) performed a similar study for upper-air observations but without subtracting a background forecast field. For a given separation in time and space, they found slightly higher correlations on isentropic surfaces than on isobaric surfaces for wind and temperature but slightly lower correlations for Montgomery streamfunction. Seaman and Gauntlett's comparison, however, was biased against the isentropic statistics in that significant-level data were not used. The PROFS study, including significant-level data and subtracting a forecast background, will be reported in a future paper. It is also noted that correlations for forecast error from the MAPS isentropic model have not yet been determined and may differ from those using NGM forecasts interpolated to isentropic coordinates.

c. *Vertical correlation of background error*

The MAPS isentropic analysis, like most operational analysis schemes, makes the separability assumption that three-dimensional correlations may be factored

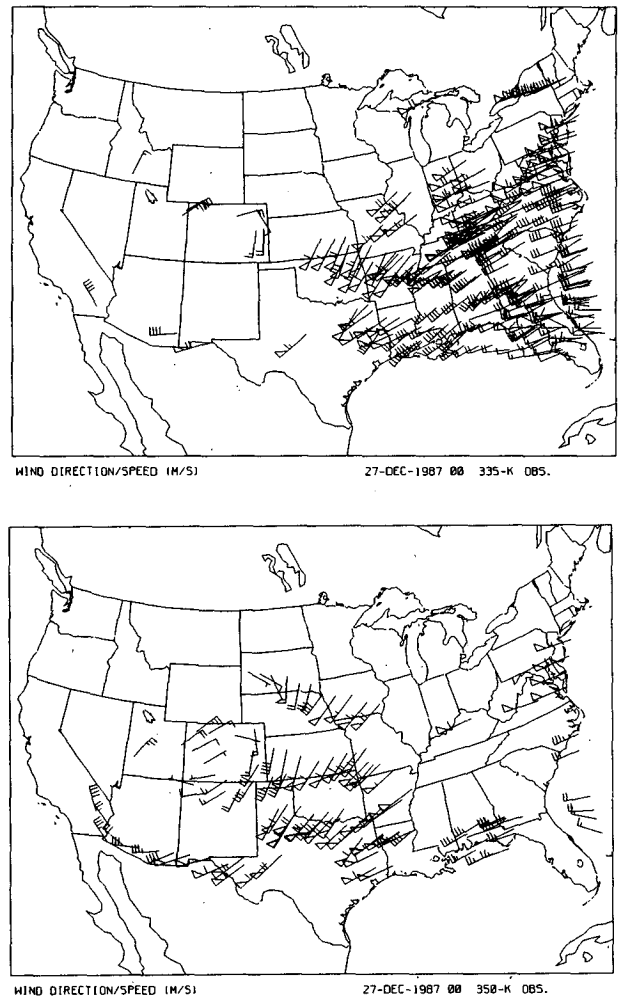

FIG. 10. Aircraft and Colorado profiler wind observations for 0000 UTC 27 December 1987. Solid flag = 50 m s^{-1}. (a) 335 K, (b) 350 K.

into the product of a horizontal and a vertical correlation. The vertical correlation in the MAPS analysis is used mostly for single-level wind reports, but also in a limited sense for surface observations of pressure and RH* at a given potential temperature. This assumption of separability is not without risk, since the true three-dimensional error structures, which the analysis attempts to reproduce, are related to the complicated 3-D structures of the atmospheric features being analyzed. There is reason to believe, however, that these errors of approximation are minimized in the isentropic framework. Most operational analysis systems determine vertical separation as a function of the log difference between two pressure levels. Here, the vertical correlation of forecast error is modeled as a function of the potential temperature difference between two levels. This approach incorporates the physical reasoning that greater differences in wind or other variables are more likely across a very stable layer of a given pressure separation than across a weakly stable layer. The Richardson number is also based on this concept. Examples of three-dimensional analysis increment structures in isentropic coordinates are shown in sections 6 and 7.

Rawinsonde data from the United States over an 8-month period were used to determine the vertical correlation of NGM 12-h forecast error of u and v components. Again, the data were fit with a three-parameter SOAR function. The u component correlations (Fig. 4) showed slightly higher values at both small and large separations, and a mean of the u and v curve-fits was used in the function for the analysis

$$\mu(\Delta\theta) = 0.32 + 0.68(1 + 0.19|\Delta\theta|)e^{-0.19|\Delta\theta|}, \quad (4)$$

where $\Delta\theta$ is in [K].

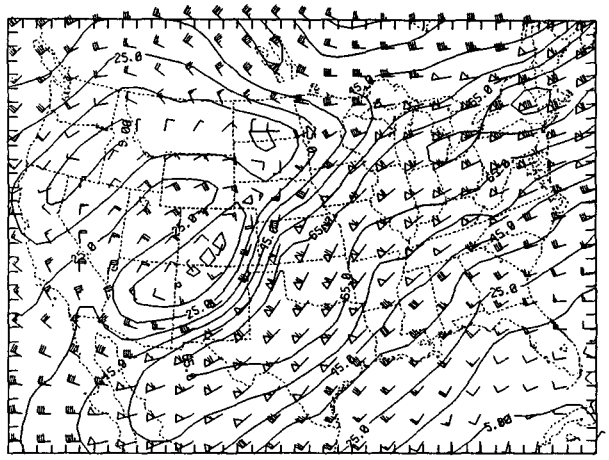

FIG. 11. Wind analysis for 335 K isentropic surface 0000 UTC 27 December 1987. Solid flag = 50 m s^{-1}.

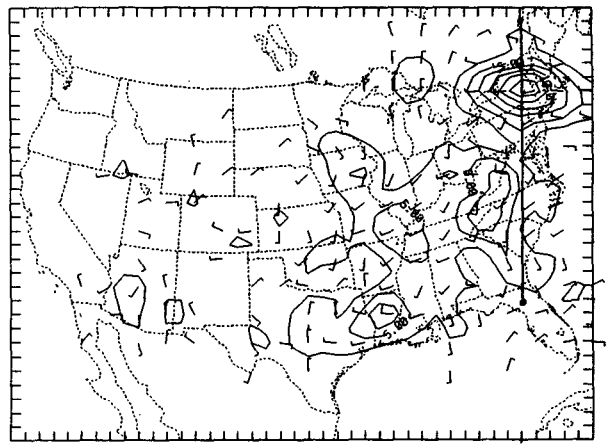

FIG. 12. Difference field between two wind analyses at 335 K, one with and one without aircraft data. Isopleths are for vector difference magnitude in m s^{-1}, contour interval = 2.5 m s^{-1}, full barb = 10 m s^{-1} (20 kt). Change vector only plotted at points with greater than 2 m s^{-1} vector difference.

5. Analysis technique

The increasingly heterogeneous nature of data on the mesoscale requires an analysis approach such as statistical interpolation that 1) combines different kinds of observation with a forecast model background, 2) accounts for errors in the background and diversity of errors in the observations, and 3) allows for variable data density.

a. Optimal interpolation analysis

A multivariate analysis of Montgomery streamfunction and winds is performed. The cross-covariances of M, u, and v are determined from the geostrophic wind relation applied to the expression for horizontal covariance of M forecast error,

$$\langle M_i' M_j' \rangle = \mu_{ij}\sigma_{M^i}\sigma_{M^j} = \mu_{ij}\sigma_M{}^2, \quad (5)$$

where $'$ signifies the residual (observation minus background), the subscripts i and j denote two different points on the same isentropic surface, μ is a correlation, and σ is a standard deviation of the forecast (background) error. The last equivalence can be made because the background error is assumed to be homogeneous.

The geostrophic wind relation in θ coordinates is

$$f\mathbf{V}_{g\theta} = \mathbf{k} \times \nabla_\theta M. \quad (6)$$

By taking partial derivatives of the M covariance expression (5), the following cross-covariances may be derived under the assumption that forecast errors of M and the horizontal wind components are geostrophically related:

$$\langle M_i' u_j' \rangle = -\frac{1}{f_j}\frac{\partial}{\partial y_j}\langle M_i' M_j' \rangle \quad (7a)$$

$$\langle M_i' v_j' \rangle = \frac{1}{f_j} \frac{\partial}{\partial x_j} \langle M_i' M_j' \rangle \quad (7b)$$

$$\langle u_i' M_j' \rangle = -\frac{1}{f_i} \frac{\partial}{\partial y_i} \langle M_i' M_j' \rangle \quad (7c)$$

$$\langle v_i' M_j' \rangle = \frac{1}{f_i} \frac{\partial}{\partial x_i} \langle M_i' M_j' \rangle \quad (7d)$$

$$\langle u_i' u_j' \rangle = \frac{1}{f_i f_j} \frac{\partial^2}{\partial y_i \partial y_j} \langle M_i' M_j' \rangle \quad (7e)$$

$$\langle v_i' v_j' \rangle = \frac{1}{f_i f_j} \frac{\partial^2}{\partial x_i \partial x_j} \langle M_i' M_j' \rangle \quad (7f)$$

$$\langle u_i' v_j' \rangle = -\frac{1}{f_i f_j} \frac{\partial^2}{\partial x_j \partial y_i} \langle M_i' M_j' \rangle \quad (7g)$$

$$\langle v_i' u_j' \rangle = -\frac{1}{f_i f_j} \frac{\partial^2}{\partial x_i \partial y_i} \langle M_i' M_j' \rangle. \quad (7h)$$

These equations are similar to the isobaric multivariate equations given by Schlatter (1975). The analytical model chosen for background forecast error correlation is the second-order autoregressive function (Thiébaux 1985); the coefficients used are listed in Table 4.

Because a full geostrophic constraint can often decrease fit of the analysis to wind observations (for instance, in ridges and troughs) and is not appropriate for a mesoscale analysis anyway, the cross-covariances between mass and winds are multiplied by a factor of 0.5 to relax the geostrophic coupling. The cross-covariances between u and v wind components are left unchanged, with the result that the wind increment field is "locally" (within the analysis volume) nondivergent. Pedder (1988) has shown that neglect of intercomponent covariances can lead to significant errors in vorticity and divergence. Divergence is permitted within the wind increment field, but only on scales larger than the 2 × 2 analysis volumes discussed in section 5b.

For pressure and RH*, a univariate analysis is performed using the observational and background errors listed in Tables 3 and 4. If coupling is required between the wind and pressure analyses, the analysis has the option of determining the pressure increment field hydrostatically from the M increment field.

b. *Observation selection strategy*

To improve computational efficiency, a limited volume method is used in the MAPS analysis whereby a fixed group of observations are selected to influence a set of four grid points at a single level. Since the PROFS computers do not have vector processors, larger volume methods such as those used at large operational centers are not advantageous. Moreover, in order to compute analyses for real-time use at PROFS, it is not even

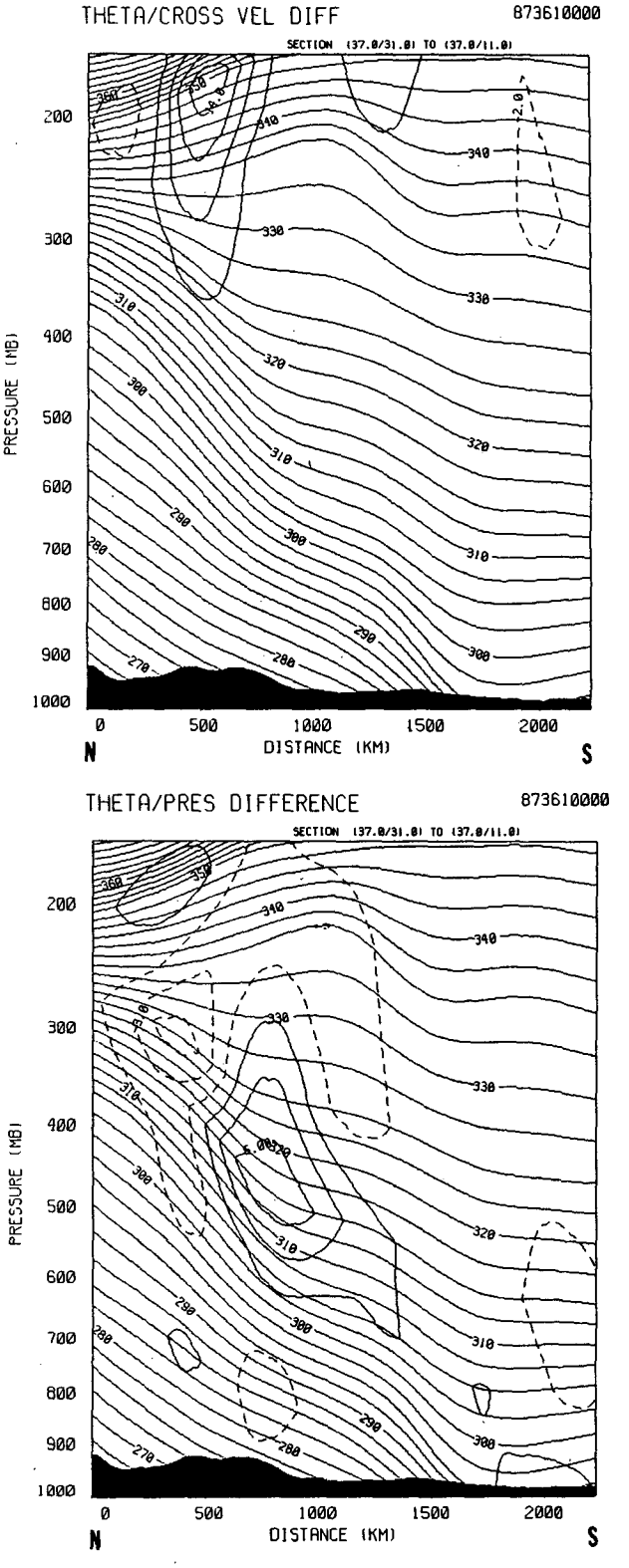

FIG. 13. Cross section of difference field between isentropic analyses with and without aircraft data. Isentropes are for analysis with all data included. (a) u component difference (contours at −2, 2, 6, 10, 14 m s^{-1}). (b) pressure displacement of isentropes (contours at −5, −3, −1, 1, 3, 5 mb). Orientation of cross section shown in Fig. 12.

possible to use larger volume methods at the current time. The "local" O/I solution in the MAPS analysis effectively truncates the correlation function, and the spectral response of the analysis increment is more noisy than if all observations were used to analyze all grid points. This behavior is discussed by Julian and Thiébaux (1975). Therefore, a light smoother–desmoother (Shapiro 1970) is used to filter the final analysis.

The maximum number of grid points that should be analyzed using the same set of observations is related to the grid length, the mean separation between observations, and the search strategy. In the MAPS scheme, the mean search radius is about 700 km, guaranteeing that there will be considerable overlap in stations chosen between adjacent groups of four points with a 111-km gridlength.

A pointer system identifies stations within each grid volume and allows the search algorithm to locate the nearest report in each of the eight search sectors shown in Fig. 5. The use of directional sectors (changed slightly from those in Benjamin et al. 1985) assures that the analysis will use observations distributed uniformly in all directions and thereby improve analyzed gradients.

The number of observations used in the multivariate analysis generally ranges between 24 and 56, 24 if a rawinsonde station is found in each sector and 56 if an additional aircraft wind report and a surface wind report closer than the rawinsonde are also found in each sector. Typically, about 40 observations per analysis volume are used in data-rich regions in the upper troposphere. For univariate analyses of pressure and RH*, up to 16 observations are used in each analysis volume.

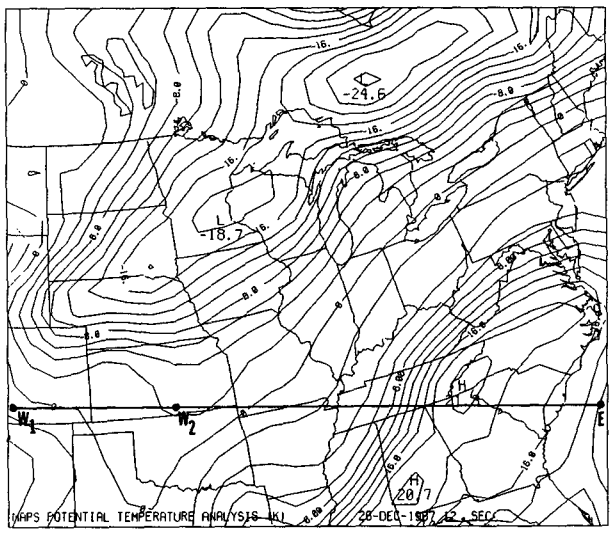

FIG. 14. Analysis of surface potential temperature from surface observations for 1200 UTC 26 December 1987. Contour interval = 2°C.

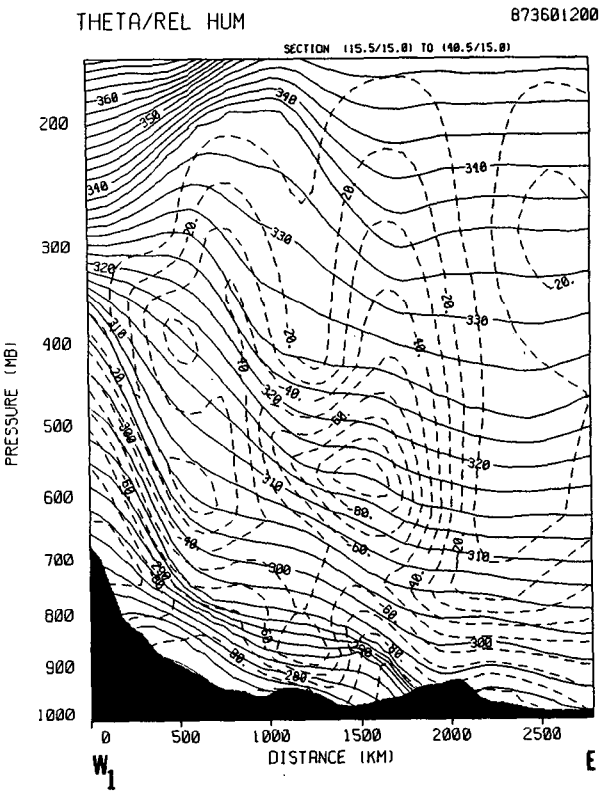

FIG. 15. Cross section of isentropes (solid) and relative humidity (dashed) for isentropic analysis with all data included for 1200 UTC 26 December 1987. Orientation of cross section shown in Fig. 14.

6. Comparisons with a pressure coordinate system

The MAPS isentropic and isobaric analyses are configured with identical specifications of observation and forecast error variances. The forecast error covariance models differ only slightly. Thus, differences between the two analyses may be attributed to the use of different vertical coordinates. Since isentropic surfaces are material surfaces along which air parcels move in the absence of diabatic processes, they are coincident with air masses which are frequently sloping layers of air. Isobaric surfaces, on the other hand, intersect these air masses rather than following them. Observations used in an isentropic analysis therefore are more likely to influence analyzed values within the same air mass as the observation and to maintain discontinuities between different air masses. The following examples demonstrate these differences.

a. Relative humidity

The first comparison illustrates the variation in spatial coherence between isentropic and isobaric coordinates, in this case, in the relative humidity field. An analysis from 1200 UTC 17 March 1987 for the 305 K surface, centered near the middle troposphere, is shown in Fig. 6a. The pressure contours for this surface

(Fig. 6b) indicate the presence of an intense cold pool coincident with a deep trough over the southwestern United States. Moisture is streaming northward to the east of this trough, and a pronounced tongue of high RH is evident from the Gulf of Mexico into the Dakotas. A second moist conveyor belt ahead of an upper-level short wave is also apparent over the Pacific Northwest. In the isobaric analysis (Fig. 6c), however, we see only the intersection of the primary moist conveyor belt with the 500 mb surface from Minnesota to Montana and no indication of the origin of the moist air.

Greater spatial coherence on isentropic surfaces is typical, in the author's experience, for advective features such as the moist tongues shown in this case. This coherence is advantageous for analysis since patterns can be better resolved with data of a given distribution. Namias (1940) discusses moisture patterns on isentropic surfaces and their forecasting applications. Even in regions of saturation where air trajectories follow constant wet-bulb potential temperature (θ_w) surfaces rather than those of constant θ, isentropic surfaces are still superior to isobaric surfaces as an approximation to the surface actually followed by air parcels.

b. Three-dimensional multivariate mass/wind analysis

A second example of isobaric versus isentropic analysis depicts the differences in three-dimensional multivariate mass/wind analysis. In this comparison, a single-level wind residual of 30 m s^{-1} out of the south at 300 mb and θ = 325 K has been assumed, and its effect on the mass analysis increment is examined. This wind residual is unusually large, chosen so that its effects are obvious. In order to consider the isentropic/isobaric difference in a baroclinic situation, the wind residual has been applied on the east side of a deep trough at 1200 UTC 26 December 1987. The effect of this hypothetical wind observation on a three-dimensional isobaric analysis is shown in Fig. 7. The horizontal forecast error correlation model valid for 325 K has been applied in both isobaric and isentropic frameworks. The vertical correlation model in the isobaric test is that reported by DiMego [1988, Eq. (6)] with k_p = 9, whereas the isentropic test (Fig. 8) uses Eq. (2) of this paper.

The vertical cross sections of the geopotential and temperature increments for the isobaric analysis (Figs. 7a–b) are both symmetrical. A horizontal cross section through the height increment field at the observation level would be similar to the $\langle v'h' \rangle$ correlation in Fig. 3 of Schlatter (1975), reflecting an increase in the west–east height gradient to be geostrophically consistent with the observed wind. The temperature increment field is determined from the vertical gradient of the height increment field. Finally, multiplying the temperature increment by the local stability gives the pres-

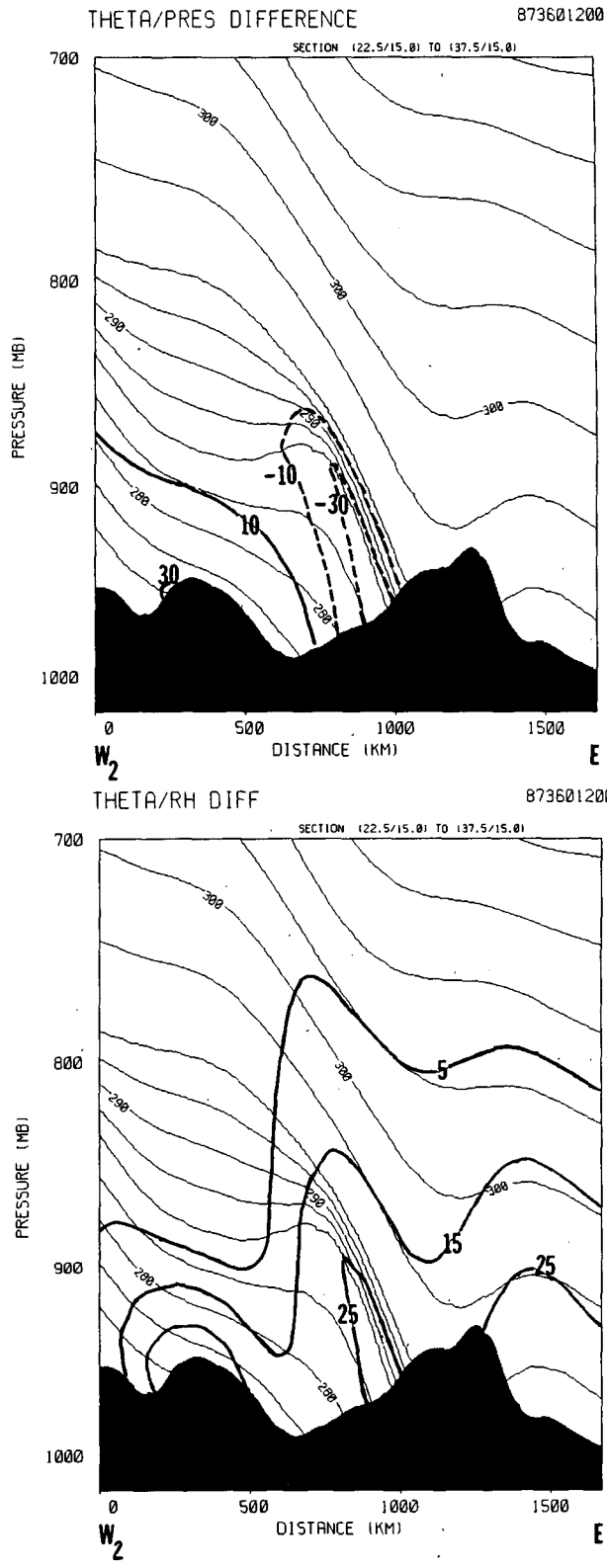

FIG. 16. Cross section of difference field between isentropic analyses with and without surface data. Isentropes are for analysis with all data included. (a) pressure displacement of isentropes (mb), (b) relative humidity difference (%).

sure increment relative to isentropic surfaces (Fig. 7c). This field shows local variations due to variations of stability in the cross section, but is still relatively symmetrical.

The three-dimensional increment fields in the isentropic system due to the single wind observation are shown in Fig. 8. The asymmetry of mass increments from the wind observation in the vicinity of a baroclinic zone is apparent in the vertical cross section of M change (Fig. 8a). This asymmetry is accentuated in the temperature and pressure increment fields (Figs. 8b–c), in which the isentropic surfaces are being stretched apart (destabilizing) on the anticyclonic side of the jet and compressed (stabilizing) on the cyclonic side of the jet.

It is significant that the isopleths of the temperature and pressure increments in the isentropic test are sloped along the frontal zone whereas those of the isobaric test are vertically stacked (equivalent barotropic). This indicates that the isentropic perspective tends to strengthen the frontal zone in its original position; the isobaric perspective, on the other hand, tends to tilt the frontal zone toward the vertical rather than tighten the isentropes within the frontal zone. This difference is a result both of performing the horizontal analysis on isentropic surfaces and of using a vertical correlation model based on potential temperature separation. Barwell and Lorenc (1985) noted the importance of distributing the influence of aircraft data vertically and introducing a consistent mass correction geostrophically. This can be accomplished in both the isobaric and isentropic systems, but the structure of these wind and mass increment fields can vary in the isentropic system in a manner consistent with the local atmospheric structure.

7. Effects of aircraft and surface observations

The effects of both types of single-level observations (aircraft and surface) on isentropic analyses will be examined for a winter storm on 26–27 December 1987.

a. Effects of aircraft observations

At 0000 UTC 27 December 1987, a deep upper-level cutoff low was positioned over the southwest United States, and a strong upper-level front stretched from Texas to New England. Weak baroclinity near the tropopause is visible in the analysis of pressure on the 335 K isentropic surface at that time (Fig. 9); the horizontal gradients of pressure on lower θ surfaces were much more intense. Many upper-level rawinsonde wind observations were missing due to blow-off from the strong jet stream (Fig. 9). A substantial number of aircraft reports were made between 2230 and 0130 UTC—254 reports between 330 and 342.5 K (Fig. 10a) and an additional 105 reports between 342.5 and 357.5 K (Fig. 10b). These data, along with reports from three profilers located over eastern Colorado included in Fig. 10, provide excellent horizontal resolution of the cutoff low over the southwestern United States and, in general, of the upper-level wind flow south of a line between San Francisco and New York.

Isentropic analyses were produced with and without aircraft data (a total of 616 reports at all levels). Wind speeds in the jet core reached 89 m s^{-1} (173 kt) near Albany, New York in the analysis including all data (Fig. 11). The vector difference field (Fig. 12) revealed that vector changes of analyzed wind of at least 2.5 m s^{-1} (5 kt) due to inclusion of aircraft data were common over the eastern half of the United States. The largest difference (17 m s^{-1}, 34 kt) was made over New England in the jet core. The change in vector wind over the southwestern United States was surprisingly small. In this region, the combined information from the 12-h NGM forecast and the rawinsonde observations was apparently already quite accurate, and the additional information from the aircraft reports had little additional effect. North–south cross sections of u-component and pressure difference were made through the zone of largest change at 335 K (Figs. 13a and 13b, respectively). The enhancement of the jet above the main frontal zone is apparent, and a slight increase of westerly momentum above a second weaker upper-level front to the south is also shown. The change in the mass field (Fig. 13b) is similar to the idealized pressure change from a single-level wind report in Fig. 8c, but the magnitude of the actual change is smaller. This is because 1) the wind increment is only half of that in the idealized case, and 2) the geostrophic decoupling reduces the effect of the winds upon the mass analysis. The orientation of the pressure change isopleths indicates, however, as it does in the idealized case, that the aircraft data, despite being single-level, are enhancing the baroclinity ($\partial\theta/\partial p$ and $\partial\theta/\partial x$) along the frontal zone beneath.

b. Effects of surface observations

Surface observations have been used before in *subjective* isentropic cross-section analyses. They are potentially useful in three-dimensional *objective* isentropic analyses for the same reasons: they can provide excellent resolution of surface fronts and other surface discontinuities. Moreover, they are strongly correlated with conditions in the lower troposphere when the surface mixed layer is deep.

In the situation just examined, cold air had spread out at the surface over most of the central United States (Fig. 14). Two cold fronts were evident in the surface potential temperature field (produced by an analysis described in Miller and Benjamin 1988), the first one blocked by the southern Appalachians. Surface potential temperatures ahead of this front, nearly 20°C, were unusually warm for a winter morning. A large-scale west-to-east cross section from isentropic analyses at

all levels shows the position of the front on the western flank of the Appalachians (Fig. 15). Air near the surface is quite moist at low levels all along this cross section, but a maximum exists at the surface front. Dry air, which has descended along the upper-level front over the western Plains, is apparent down to 600 mb.

To show the effects of surface observations, the cross section is zoomed (Fig. 16a) to the section close to the surface position of the front. Isentropic analyses were performed with and without surface observations. The difference in the pressure analysis (Fig. 16a) shows that the surface data have caused the analysis to sharpen the front by cooling the air (decreasing pressure on a given isentropic surface) immediately behind the front. The surface data have also caused a slight warming (increase of pressure) farther behind the front.

The vertical influence of surface data is effectively truncated when the potential temperature difference is greater than 10 K. Thus, the depth (in pressure or height coordinates) of the layer through which surface data have influence is a function of the low-level stability. This effect is clearly shown in a cross section of the change in relative humidity produced by surface data (Fig. 16b). In this small region, the effect of surface data is to increase relative humidity everywhere with the largest increase occurring in the immediate vicinity of the surface front. This increase is consistent with the local lifting expected along the frontal zone. Another maximum in increase of RH is present farther back in the cold air over the Ozarks, 700 km west of the surface front position in the cross section. This alteration, however, does not extend through as deep a layer because of strong low-level stability. Thus, in the isentropic framework with vertical influence governed by potential temperature separation, surface observations can be used beneficially in a three-dimensional analysis resulting in physically plausible variations in their vertical influence.

8. Conclusions

An isentropic analysis scheme has been described which accommodates a wide variety of data and accounts for the expected accuracy of each kind when combining with a forecast background field. The statistical analysis scheme used here also accounts for variable data density, increasingly a characteristic of the heterogeneous observations produced around the world and in the United States.

Because this analysis operates on isentropic surfaces, it takes advantage of the long-recognized observation that fields appear more coherent on isentropic than on isobaric surfaces. This follows from the fact that adiabatic flow in the atmosphere remains on the same isentropic surface. Therefore, isentropic analysis is advantageous on the mesoscale since it enlarges the apparent scale of frontal features and features of advective origin (e.g., dry tongues, moist plumes or conveyor belts, stratospheric intrusions). The isentropic framework is helpful for quality control for the same reasons that it is helpful in analysis.

Statistics have been collected for the correlation of forecast error along isentropic surfaces for different variables. These statistics were used to develop the models for horizontal and vertical correlations that are used in the isentropic analysis.

The analysis is two-dimensional with respect to profile data (rawinsonde and wind profiler) and three-dimensional with respect to single-level data (aircraft and surface). Prescribing vertical correlation models as a function of potential temperature difference ensures that these observations produce three-dimensional analysis increment structures that are physically reasonable. The nature of these increment structures is also due, in part, to the isentropic coordinate system itself, and it is quite possible that vertical coupling is less essential in isentropic than in isobaric coordinates for the reasons described above. Aircraft and surface observations made a substantial difference in analyses because they provide higher horizontal resolution than the rawinsonde network.

The MAPS isentropic analysis is a part of an isentropic mesoscale data assimilation system with an update cycle of 3 hours which has been developed at the Program for Regional Observing and Forecasting Systems. A new domain for the isentropic analysis/forecast system at PROFS is currently being implemented. It covers a slightly larger area using a 62×48 grid with an 80-km gridlength and has 18 levels with a 6 K resolution through most of the troposphere. Reports will be made on the performance of the 3-h MAPS isentropic assimilation system in the near future.

Acknowledgments. The development of the isentropic Mesoscale Analysis and Prediction System at PROFS has been a group effort. Keith Brewster developed the objective quality control schemes, and Brian Jewett developed the subjective quality control interactive system. Tracy Lorraine Smith has been the major contributor to data ingest programs. Tom Schlatter, Rainer Bleck, Michael Pedder and John Smart were helpful in giving critical reviews of this manuscript. Tom Schlatter, Ron McPherson, Renate Brümmer, and Ralph Petersen provided insightful discussions which aided the development of the scheme. Renate Brümmer and Rainer Bleck wrote the original version of the cross-section routine used here. Hope Hamilton provided word processing assistance.

The PROFS Exploratory Development Facility branch has developed the computer infrastructure through which the observations and NMC data are accessible. Delta Airlines and United Airlines were most cooperative in making their aircraft data available to PROFS for development of our analysis and assimilation system.

REFERENCES

Andersson, E., N. Gustaffson, L. Meuller and G. Omstedt, 1986: Development of mesoscale analysis schemes for nowcasting and very short-range forecasting. SMHI Promis-Rapporter No. 1, Swedish Meteorological and Hydrological Institute, Norrköping, Sweden, 75 pp.

Anthes, R. A., and D. P. Baumhefner, 1984: A diagram depicting forecast skill and predictability. *Bull. Amer. Meteor. Soc.*, **65**, 701–703.

——, Y.-H. Kuo, S. G. Benjamin and Y.-F. Li, 1982: The evolution of the mesoscale environment of severe local storms: preliminary modeling results. *Mon. Wea. Rev.*, **110**, 1187–1213.

Barwell, B. R., and A. C. Lorenc, 1985: A study of the impact of aircraft wind observations on a large-scale analysis and numerical weather prediction system. *Quart. J. Roy. Meteor. Soc.*, **111**, 103–129.

Benjamin, S. G., R. S. Lieberman, T. W. Schlatter and R. G. Rasmussen, 1985: Preliminary tests of a regional objective analysis and short-range numerical forecasting system. Preprints, *Seventh Conference on Numerical Weather Prediction*, Montreal, Amer. Meteor. Soc., 440–443.

——, D. L. Birkenheuer, R. D. McPherson, T. L. Smith and J. S. Snook, 1988: Experiments in the assimilation of radiance observations from VAS. Preprints, *Eighth Conference on Numerical Weather Prediction*, Baltimore, Amer. Meteor. Soc., 269–276.

Bleck, R., 1975: An economical approach to the use of wind data in the optimum interpolation of geo- and Montgomery potential fields. *Mon. Wea. Rev.*, **103**, 807–816.

——, and M. A. Shapiro, 1976: Simulation and numerical weather prediction framed in isentropic coordinates. *Weather Forecasting and Weather Forecasts: Models, Systems, and Users*, Vol. 1. NCAR Colloquium, National Center for Atmospheric Research, 154–168.

Brümmer, R., 1987: An isentropic coordinate model used in a mesoscale data assimilation system. *Symposium on Mesoscale Analysis and Forecasting*, Vancouver, Nowcasting, Intl. Asso. of Meteor. and Atmos. Phys. (IAMAP), European Space Agency SP-282, 561–564.

Buzzi, A., A. Trevisan and E. Tosi, 1985: Isentropic analysis of a case of Alpine cyclogenesis. *Beitr. Phys. Atmos.*, **58**, 273–284.

Carlson, T. N., 1980: Airflow through midlatitude cyclones and the comma cloud pattern. *Mon. Wea. Rev.*, **108**, 1498–1509.

Danielsen, E. F., 1959: The laminar structure of the atmosphere and its relation to the concept of a tropopause. *Arch. Meteor. Geophys. Bioklim.*, **A11**, 293–332.

——, and R. Bleck, 1967: Moist isentropic flow and trajectories in a developing wave cyclone. Rep. No. 67–0617, Air Force Cambridge Research Lab., Bedford, MA, 34 pp. [NTIS AD 670 847.]

Derber, J. C., 1987: Variational four-dimensional analysis using quasi-geostrophic constraints. *Mon. Wea. Rev.*, **115**, 998–1008.

Dey, C. H., and L. L. Morone, 1985: Evolution and performance of the National Meteorological Center global data assimilation system: January 1982–December 1983. *Mon. Wea. Rev.*,**113**, 304–318.

DiMego, G. J., 1988: The National Meteorological Center Regional Analysis System. *Mon. Wea. Rev.*, **116**, 977–1000.

Gandin, L. S., 1963: *Objective Analysis of Meteorological Fields.* Gidrometeorologicheskoe Izdatel'stvo, Transl. Russian 1965, 242 pp.

Julian, P. R., and H. J. Thiébaux, 1975: On some properties of correlation functions used in optimum interpolation schemes. *Mon. Wea. Rev.*, **103**, 605–616.

LeDimet, F.-X., and O. Talagrand, 1986: Variational algorithms for analysis and assimilation of meteorological observations: theoretical aspects. *Tellus*, **38A**, 97–110.

Lönnberg, P., and A. Hollingsworth, 1986: The statistical structure of short-range forecast errors as determined from radiosonde data. Part II: The covariance of height and wind errors. *Tellus*, **38A**, 135–161.

Mancuso, R. L., R. M. Endlich and L. J. Ehernberger, 1981: An objective isobaric/isentropic technique for upper air analysis. *Mon. Wea. Rev.*, **109**, 1326–1334.

Miller, P. A., and S. G. Benjamin, 1988: A scheme for analyzing surface observations over heterogeneous terrain. Preprints, *Eighth Conference on Numerical Weather Prediction*, Baltimore, Amer. Meteor. Soc., 178–184.

Namias, J., 1940: *An Introduction to the Study of Air Mass and Isentropic Analysis.* Amer. Meteor. Soc., 232 pp.

Pedder, M. A., 1988: On the influence of map analysis formulation in the estimation of wind field derivatives. *Quart. J. Roy. Meteor. Roy.*, **114**, 241–257.

Petersen, R. A., 1986: Detailed three-dimensional isentropic analysis using an objective cross sectional approach. *Mon. Wea. Rev.*, **114**, 719–735.

Rasmussen, R. G., 1982: Some techniques for the objective analysis of humidity for regional scale numerical weather prediction. NCAR/CT-67, Drexel University and National Center for Atmosphere Research, Boulder, CO, 366 pp.

Reed, R. J., and F. Sanders, 1953: An investigation of the development of a mid-tropospheric frontal zone and its associated vorticity field. *J. Meteor.*, **10**, 338–349.

Rossby, C.-G., 1937: Isentropic analysis. *Bull. Amer. Meteor. Soc.*, **18**, 201–209.

Rutherford, I. D., 1972: Data assimilation by statistical interpolation of forecast error fields. *J. Atmos. Sci.*, **29**, 809–815.

Sanders, F., 1955: An investigation of the structure and dynamics of an intense surface frontal zone. *J. Meteor.*, **12**, 542–552.

Schlatter, T. W., 1975: Some experiments with a multivariate statistical objective analysis scheme. *Mon. Wea. Rev.*, **103**, 246–257.

Seaman, R. S., and F. J. Gauntlett, 1982: A quantitative comparison of variations on isobaric and isentropic surfaces in the Australian region. *Aust. Meteor. Mag.*, **30**, 273–277.

Shapiro, M. A., and J. T. Hastings, 1973: Objective cross section analysis by Hermite polynomial interpolation on isentropic surfaces. *J. Appl. Meteor.*, **12**, 753–762.

Shapiro, R., 1970: Smoothing, filtering and boundary effects. *Rev. Geophys. Space Phys.*, **8**, 359–387.

Thiébaux, H. J., 1985: On approximations to geopotential and wind-field correlation structures. *Tellus*, **37A**, 126–131.

——, H. L. Mitchell and D. W. Shantz, 1986: Horizontal structure of hemispheric forecast error correlations for geopotential and temperature. *Mon. Wea. Rev.*, **114**, 1048–1066.

Uccellini, L. W., R. A. Petersen, K. F. Brill, P. J. Kocin and J. J. Tuccillo, 1987: Synergistic interactions between an upper-level jet streak and diabatic processes that influence the development of a low-level jet and a secondary coastal cyclone. *Mon. Wea. Rev.*, **115**, 2227–2260.